Journal Pre-proof

New advanced SiC-based composite materials for use in highly oxidizing environments: synthesis of $SiC/IrSi_3$

Antonio Daniel Camarano, Donatella Giuranno, Javier Narciso

PII: S0955-2219(19)30690-9

DOI: https://doi.org/10.1016/j.jeurceramsoc.2019.10.018

Reference: JECS 12780

To appear in: *Journal of the European Ceramic Society*

Received Date: 5 May 2019

Revised Date: 5 October 2019

Accepted Date: 10 October 2019

Please cite this article as: Camarano AD, Giuranno D, Narciso J, New advanced SiC-based composite materials for use in highly oxidizing environments: synthesis of $SiC/IrSi_3$, *Journal of the European Ceramic Society* (2019), doi: https://doi.org/10.1016/j.jeurceramsoc.2019.10.018

New advanced SiC-based composite materials for use in highly oxidizing environments: synthesis of $SiC/IrSi_3$

Antonio Camarano[1], Donatella Giuranno[2*], Javier Narciso[1,*]

Antonio Daniel Camarano[1]: antoniodaniel.camarano@ua.es
Donatella Giuranno[2*], corresponding author email: donatella.giuranno@ge.icmate.cnr.it,
Javier Narciso[1]: corresponding author email: narciso@ua.es

Affiliations:

[1] Instituto Universitario de Materiales de Alicante (IUMA), Universidad de Alicante, Apdo. 99, Alicante, 03080, Spain

[2]Institute of Condensed Matter Chemistry and Energy Technologies (ICMATE), National Research Council of Italy (CNR),Via De Marini 6, Genoa, 16149, Italy

Abstract

Currently, MMCs with SiC as reinforcement emerge as ideal candidates for long-term stable devices withstanding high temperatures and harsh operating environments which are typical for many industrial sectors, such as energy, aerospace, electronics, catalysis, etc. However, the costly manufacture of such composites is the major restraint to make them marketable.

In this paper, highly-dense, nearly-shaped $SiC/IrSi_3$ composites effortless produced at T = 1250°C under a vacuum by reactive melt infiltration of liquid Si-62wt%Ir eutectic alloy into bimodal SiC_p-C porous preforms, are presented. The replacement of unreacted detrimental Si by a tougher and less oxidizing intermetallic phase ($IrSi_3$) was successfully obtained.

Keywords: MMCs; Silicon Carbide; Ir-silicides; Reactive infiltration;Oxidizing atmosphere.

1. Introduction

The future of composite materials is extremely bright. In particular, advanced composites will dominate in almost any industrial sector. Aerospace industry and energy production are just two of the many market segments that will see a large increase in the use of ad-hoc designed materials, with outstanding performance and long-term stability in operating at high temperature and oxidizing environments.

To date, metal-matrix (MMCs) and ceramic-matrix composite materials (CMCs), in particular SiC-based composites, meet the aforementioned requirements [1, 2], because the combination of their outstanding features, such as excellent thermo-mechanical properties, high wear resistance and remarkable chemical stability in corrosive-oxidizing environments [3, 4].

Whether SiC is the matrix or present as reinforcing phase, it is a refractory material with excellent properties strictly related to the strong covalent bond between Si and C. However, a so strong covalent bond also represents an inconvenient in the SiC-synthesis and production. Indeed, owing to low self-diffusion coefficient, by using conventional sintering process, it is very difficult to obtain compact or at least highly dense SiC (reduced porosity). Moreover, sintered SiC is a costly product manufactured in limited simple geometries cause the severe operating conditions required (> 1800°C, 10-40 MPa) [5-9]. In order to solve these technological limitations, alternative processes have been proposed and developed such as reactive infiltration [10-12] and chemical vapor infiltration (CVI) [13-15]. In particular, the reactive infiltration of carbon (C) or SiC-based preforms by liquid silicon (Si), named Reaction Bonded Silicon Carbide (RBSC), allows to fabricate highly-dense, shaped and cost-less SiC at lower temperatures (1450–1600°C) than the conventional ones, and without applying any external pressure or using additives [16–19]. Despite these advantages, the main drawback of these products is the presence of unreacted Si (5-25vol%) compromising the overall mechanical performance of the composite. The replacement of such metal phase with intermetallic compounds (silicides) like $MoSi_2$ [20], WSi_2 [21], $CoSi_2$ [22,23] or $ZrSi_2$ [24], has recently gained attention in developing structural composites as candidates for extremely high-temperature applications. As demonstrated, the mentioned composites, easily manufactured by reactive infiltration, were exhibiting good thermo-mechanical performance and microstructural long-term stability combined with improved oxidation resistance [25].

In this context, even if limited to some "niche" applications, Iridium (Ir) and Ir-silicides arise as new and suitable alternative constituents worthy to be investigated as Si-replacement phase in RBSC process. In fact, Ir exhibits a unique set of properties almost meeting the key requirements in a wide range of highly demanding applications [26], such as the high melting temperature (2446°C) [27], high specific strength at high temperature, remarkable oxidation and corrosion resistance. To now, Ir is already used in catalysis [28, 29], to manufacture high temperature crucibles, for dental implants and jewellery, for sensors [30] and electronic devices working at high temperatures (dimensionally stable anodes) [31]. Ir is used also as hardening agent for other metals, (such as Pt [32]) and multicomponent alloys [33]. As reported by [34, 35], in its massive state, Ir is not soluble in acids, salts, does not reacts with C to form carbides, shows negligible C-solubility and it is virtually impenetrable by oxygen up to T = 2370°C. Therefore, Ir is successfully used as coating material for various substrates acting as a chemically stable oxygen diffusion barrier even at high temperature [36-37]. Similarly, Ir-Si system and Ir-silicides, show improved thermo-mechanical properties [38]. Regarding oxidation, it should be noted that the literature is really scarce, but nonetheless it indicates that oxidation resistance is significantly improved with

the presence of silicides [39-41]. It is because, within the oxidation process of silicides, SiO_2 is resulting as unique oxidation product instead of both oxides As a consequence of the diffusion of Si through the crystalline network (and not oxygen) [42, 43], an enrichment of Ir in the silicide phase is promoted. . Additionally, going back to composites, the Si, Ir and SiC coefficients of thermal expansion (CTE) [44-46], are almost comparable. The thermal-compatibility among the constituent phases is crucial in predicting, in a composite material, catastrophic failure caused by thermal expansion mismatch.

In this paper, the synthesis of highly dense SiC/$IrSi_3$ composite materials by reactive infiltration of liquid Si-62wt%Ir eutectic alloy (Si-19.5at%Ir) [47] into bimodal SiC_p-C preform is presented as main achievement. In particular, SiC/$IrSi_3$ were cost-less obtained at T = 1250°C and under a vacuum. In addition, a careful analysis of infiltration kinetics as a function of the current operating conditions, interfacial phenomena observed and related microstructure development was performed. In order to evaluate the viability of the selected route, the results obtained are compared with those of produced SiC/Si composite material by applying the same procedure.

2. Experimental details

2.1. Materials

The SiC-C preforms used in this work were kindly provided by Petroceramic [48] as plates with dimensions of 25x25x5 mm. These preforms consist of a bimodal mixture of α-SiC particles (SiC_p), with particle sizes of 36.5 and 4.5 μm, incorporated into a C-matrix. SiC_p-C preforms were prepared by mechanically mixing α-SiC_p with phenolic resin (10 wt%). The mixture was uniaxially pressed under a P = 140 MPa and at T = 150°C with resulting melt of the resin was melted and a strong cross-linking between α-SiC particles. The obtained green body was subsequently pyrolyzed under a N_2 atmosphere at T = 700ºC. During pyrolysis, the resin turned into C and a porosity was created inside the sample due to gas releasing of volatile products. Prior to the experiments, the SiC_p-C preforms (12x12x3 mm) were further thermally treated up to T = 1500°C to remove residual volatile compounds. In Table 1, the results of the characterization of the SiC_p-C preform used in this work are detailed. A detailed description of the characterization techniques used can be found in previous articles of the research group [49, 50].

Tab. 1. Results from the characterization of the SiC_p-C Petroceramic preforms.

The apparent density and He-density were accurately measured. As a result of three different measurements, apparent density in the range of 2.10-2.20 g/cm^3 and a He-density of 3.10 g/cm^3

were obtained, resulting in a porosity range of 29-32.3 % Additionally, by Hg-porosimetry technique, the pore size and the porous distribution were determined (see Table 1). In Table 1 the composition of each constituent is also reported. The composition was determined by thermo-gravimetric analysis (TGA) technique, under an oxidant atmosphere (N_2/O_2, 4/1) in the range of T = 25-900ºC. The role of C is twice: as binder and as reactant/precursor in the production of additional SiC during reactive infiltration with liquid Si or Si-based alloys. In Figure 1, the microstructure and composition of the as received SiC_p-C preform, analyzed by SEM/EDS and X-ray diffraction, respectively are shown. By SEM analysis, two granulometries of SiC particles are well distinguished (light gray) as well as the C phase surrounding the SiC particles (black). As resulting by XRD analysis, α-SiC (as a mixture of the 4H and 6H polytypes) is the only crystalline phase detected in the preform.

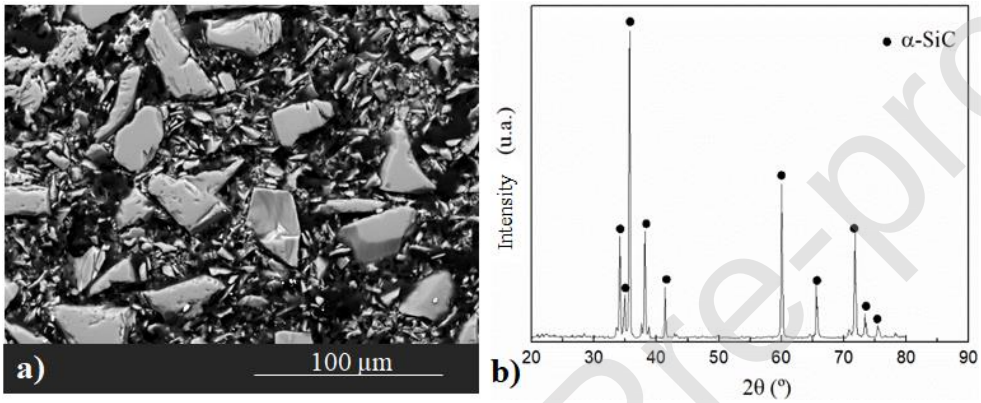

Fig. 1. As received SiC_p-C preform: a) Secondary electron micrograph after polishing and b) XRD pattern.

The Si-62wt%Ir alloy samples (from now Si-Ir eutectic alloy), eutectic composition, were prepared by mixing high purity Ir and Si (99.98%-Goodfellow®). Eutectic alloy samples were produced with a weight of 50.0 mg for infiltration experiments. The alloy samples were produced by arc melting technique under an atmosphere of Ar (N60, O_2 < 0.1 ppm). Before the arc melting of Ir-Si alloys, the residual oxygen content inside the chamber was reduced by melting a Zr drop. To ensure the homogeneity of the alloy composition, the melting of every single Ir-Si sample was repeated 3 times. The as produced Ir-Si composition was checked on cross-sectioned sample both by SEM (to reveal eutectic microstructure) and XRD (to detect the phases) as shown in Figure 2.

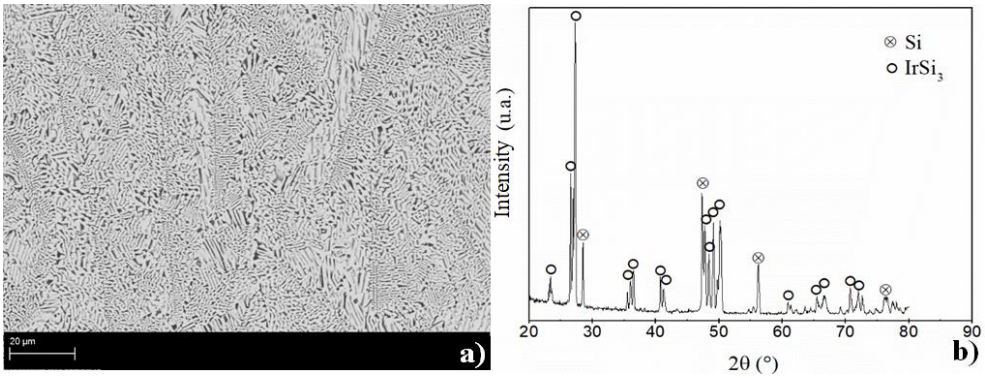

Fig. 2. As-produced Si-62wt%Ir eutectic alloy by arc melting: a) SEM image at the cross-section and b) XRD pattern

2.2 Procedure and method

The goal of this experimental work is the study of the infiltration kinetics of both liquid Si and Si-Ir eutectic alloy into SiC_p-C porous preforms (see section 3). For infiltration experiments, an induction horizontal furnace was used and extensively described elsewhere [23, 43].

Prior to the experiments, the metal sample was rinsed in ethanol and ultrasonicated, the residual powder from the SiC_p-C preform was removed by compressed air.

At room temperature the Si/SiC_p-C and Si-Ir eutectic alloy/SiC_p-C couples were placed on a graphite plate/sample holder, introduced into the furnace and located at the central part of the heater. Once leveled the sample at horizontal plane, in order to remove any contaminant from the experimental environment, the chamber was degassed under a vacuum (down to 10^{-4} Pa) for two hours.

In order to promote the reactive infiltration and to decrease the resulting porosity, the procedure suggested by [49, 50] was applied. The metal sample/substrate couple was heated under a vacuum by a 800 kHz high frequency generator coupled to a graphite susceptor ensuring an experimental surrounding atmosphere with reduced oxygen content ($PO_2 < 10^{-6}$ Pa). During all the experiments, the oxygen partial pressure was measured by an oxygen sensor [51] and the temperature was monitored by a pyrometer, previously calibrated by detecting the melting temperature of high purity metals (Sn, Al, Au, Cu, Si and Ni).

The infiltration experiments were performed by contact heating sessile drop method. The temperature was risen up to the testing temperature with a rate of 5°C/s. The selected temperature was kept constant until the complete infiltration of the preform, then the samples were quenched (cooling rate 10°C/s) to preserve the new formed interfaces and infiltrated microstructure. The evolution of infiltration experiments was monitored in real time and recorded (10 frames/sec) by a high resolution camera connected to a computer with an image analysis software ad hoc-

developed (ASTRAVIEW®) [52]. The software allows the automatic acquisition of contact angles and drop geometric variables in real time (R-base radius and H-height). By analyzing such geometric variables as a function of time, is possible to follow the kinetics of infiltration with a great accuracy.

Owing to the different melting temperatures [47], (T = 1414°C for pure Si and T = 1222°C for Si-Ir eutectic alloy), different isothermal conditions for Si and Si-Ir eutectics infiltration experiments into SiC_p-C preforms were selected. Specifically, the testing temperature of T = 1450°C for Si/SiC_p-C and temperatures of T = 1250°C and T = 1350°C for the Si-Ir eutectic alloy/SiC_p-C, were imposed. At the end of the infiltration experiments, the samples were removed from the furnace, embedded into epoxy resin, cross-sectioned and metallographically mirror polished for microstructural characterization by SEM/EDS and XRD techniques.

3. Results and discussion

As already introduced, the present study aims to identify the mechanism mainly governing the infiltration of SiC_p-C preforms: either driven by chemical reaction or by fluido-dynamics. Firstly, it is important to note that infiltration of SiC_p-C preforms with both metal materials, pure Si and Si-Ir eutectic alloy, took place spontaneously and the complete infiltration of SiC_p-C preforms was rapidly achieved. On the other hand, since the C content in this preform is quite low (4.7 wt%), porosity and pore diameter should not substantially change during infiltration.

In order to define the main driving force governing infiltration, a careful analysis of infiltration kinetics is necessary to be performed. As reported by [53], the infiltration kinetics can be analyzed by following the evolution of the height of infiltration (*h inf*) (i.e. infiltration depth), usually described by linear, parabolic or other laws [54, 55]. It is possible to calculate *h inf* by assuming that a spherical cap geometry of the molten drop is preserved during infiltration process. This basic assumption enables to analyze the infiltration kinetics by simply following the behaviors of contact angles and drop geometrical parameters such as the drop base radius (*R*) and the h-drop height (*h*) as a function of time (see Figure 4). By using the following equation 1, it is easy to calculate the emerging drop volume (*V*) as a function of time.

$$V = \frac{\pi h}{6}(3{R_B}^2 + h^2) \qquad (1)$$

By knowing the initial volume of the drop (V_0), the infiltrated volume (V_{Inf}), can be calculated as:

$$V_{Inf} = V_0 - V \qquad (2)$$

Similar infiltration studies on C/Al-Si [55] and C/Ni-Si [56] systems are reported in literature, where the abovementioned description and interpretation of the results was applied.

In particular, this model describes the infiltrated volume accordingly to a shape of a truncated cone (as shown in Figure 3), where the bottom diameter takes a flat shape, which corresponds to the drop base diameter at the beginning of the infiltration process ($D_0 = 2R_0$). In addition, the upper diameter of the infiltrated area is equal to the final base diameter ($D_f = 2R_f$).

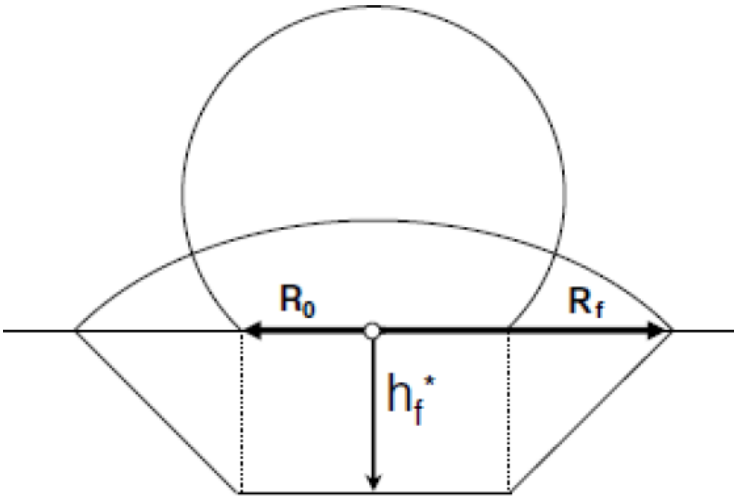

Fig. 3. Schematic drawing of the drop with the infiltrated area at the beginning and at the end of the infiltration process [55, 56].

According to equations describing a truncated cone and knowing material porosity (α_{ef}), the infiltration height (h_{Inf}) can be calculated as a function of time as follows:

$$h_{Inf}(t) = \frac{1}{\alpha_{ef}}\left(\frac{3\,V_{Inf}}{\pi\,(R^2 + {R_0}^2 + RR_0)}\right) \quad (3)$$

As mentioned above, the infiltration experiments were performed on SiC_p-C preforms, by infiltrating pure Si at T = 1450°C and Si-Ir eutectic alloys at T = 1250°C and T = 1350°C, as shown in Figure 4. The evolution of advancing contact angle and drop geometric parameters (H-drop height and R-drop base radius) are reported from the drop melting until its complete infiltration into SiC_p-C porous preforms.

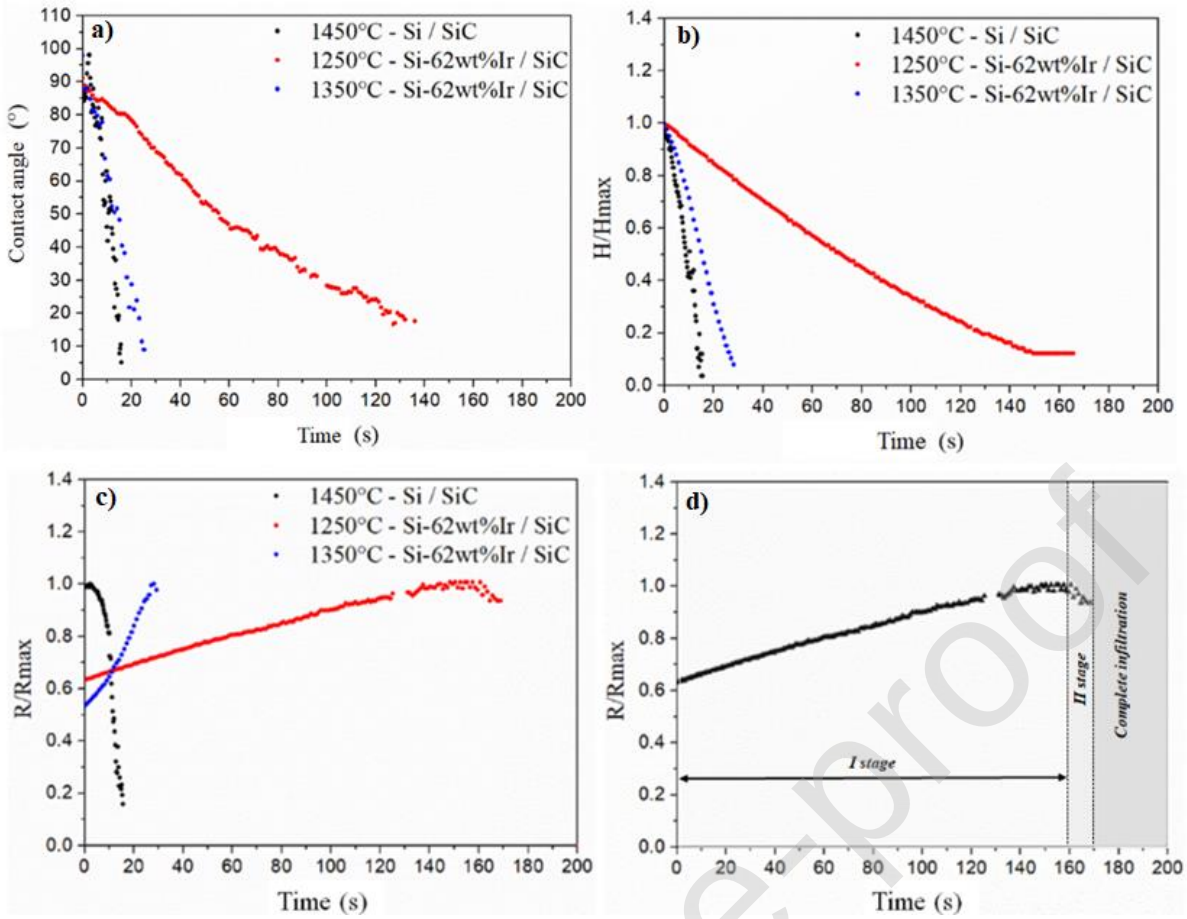

Fig. 4. Evolution of contact angles and drop geometric variables (R-drop base radius and H-drop height) recorded within the infiltration experiments performed on SiC_p-C/Si at T = 1450°C and SiC_p-C/Si-Ir eutectic alloy at T = 1250°C, 1350°C; a) evolution of contact angle, b) evolution of normalized drop height and c) evolution of normalized base radius, d) stages in the evolution of the normalized base radius.

At a first glance, the infiltration of SiC_p-C by pure Si (at T ≈ Tm + 30°C) occurred faster (one order of magnitude) than Si-Ir eutectics at T = 1250°C (≈ 30°C above the melting point). As expected, the temperature strongly influenced the infiltration process , since the increase of 100°C in the testing temperature (at T = 1350°C, see Figure 4a and 4b) substantially increases of ~ 7 times the infiltration time required for the complete infiltration: t = 25 sec at T = 1350°C and t = 170 sec at T = 1250°C. In addition, 2 stages are well distinguished in the infiltration kinetics (see Figure 4d). Within the first (I stage), the drop radius increased up to a maximum value due to capillary forces and consequently an enlargement of the infiltration front in terms of R ($R_0 < R < R_{fl}$) was observed where $R_{MAX} = R_{fl}$. At the maximum value of drop radius, a second phenomenon is observed (II stage), where the radius decreased progressively due to the appearance of hydrodynamic action [57]. Interactions between the molten drop and the porous substrate strongly influence the kinetics of each stage. Several studies performed on metal infiltration into porous substrates [58, 59] already reported about the presence of two competitive processes observed during the first stage: drop spreading process and infiltration process, as shown in Figure 5.

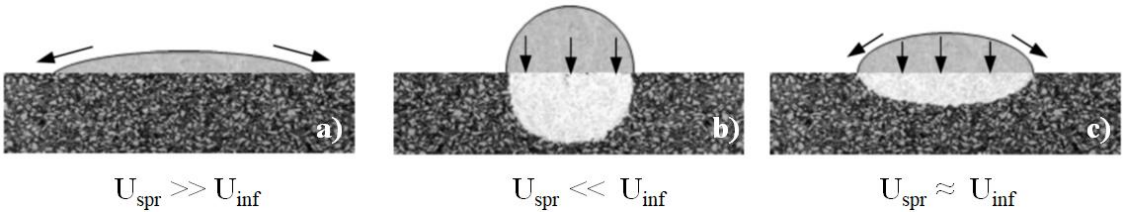

Fig. 5. Scheme of competition between spreading and infiltration and related shape of the drop during infiltration process. U_{spr} = spreading rate and U_{inf} = infiltration rate.

In Figure 6, as further evidence, the time sequence for the mentioned infiltration experiments, by collecting the more significant recorded images, is shown. It is important to highlight that molten drops preserved a regular spherical cap shape through all the infiltration process. Moreover, the kinetics of spreading clearly varied upon the infiltrating material and temperature. In the case of the Si-infiltration, absence of drop spreading was observed ($U_{spr} << U_{inf}$ case b, as shown in Figure 5).

On the contrary, analyzing the alloy behavior, the competition between spreading and infiltration is more pronounced ($U_{spr} \approx U_{inf}$ case c, as shown in Figure 5) since the maximum radius is higher than the initial equatorial one.

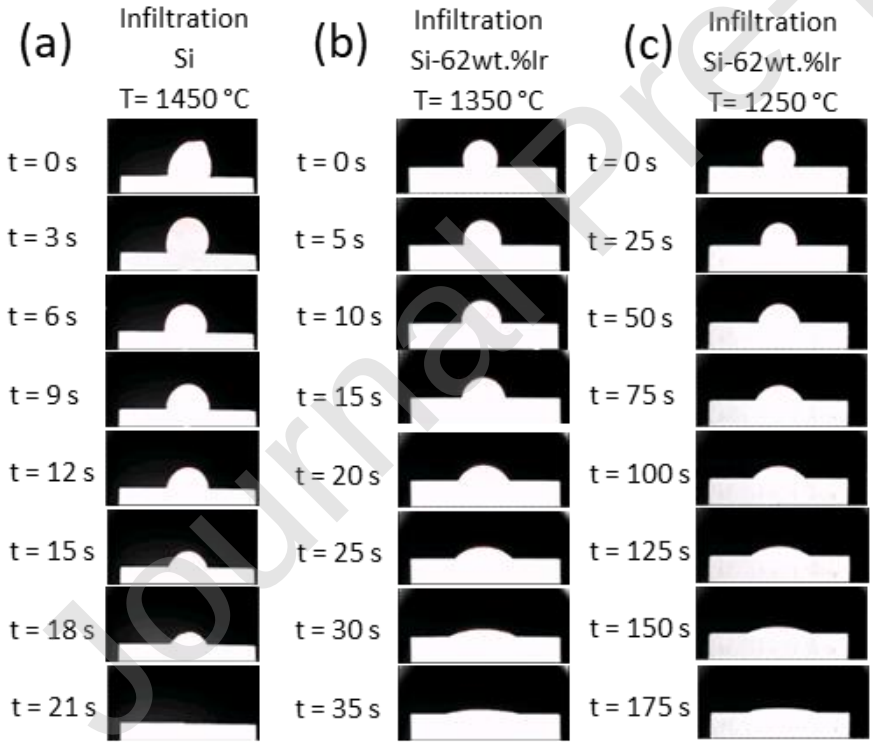

Fig. 6. Images of drop profiles recorded during infiltration experiments performed on SiC_p-C preforms with: a) Si at T = 1450°C, b) Si-Ir eutectic alloy at T = 1350°C and c) Si-Ir eutectic alloy at T = 1250°C.

In order to well interpret the different behaviors observed, a study of infiltration kinetics was carried out using the model presented in equation 3. Figure 7 shows the evolution of emerging drop volume (V), infiltrated volume (V_{inf}) and height of infiltration (h_{inf}) as a function of the

experimental conditions. As it can be seen, infiltration kinetics ($h_{inf}(t)$) are well described by linear equation, thus deviating from the Darcy's parabolic law [60, 61]. In the experiment carried out with pure Si at T = 1450°C, a weak deviation from linearity was observed within the first 3 seconds, cause the drop movements during the melting (see time sequence reported in Figures 6a and 7a) and delay in taking its spherical shape, mainly due to the presence of a layer of native SiO_2 oxide. The agreement between infiltration kinetics and linear law description of the phenomenon, is typical of interactions process mainly dominated by chemical reaction [60-62].

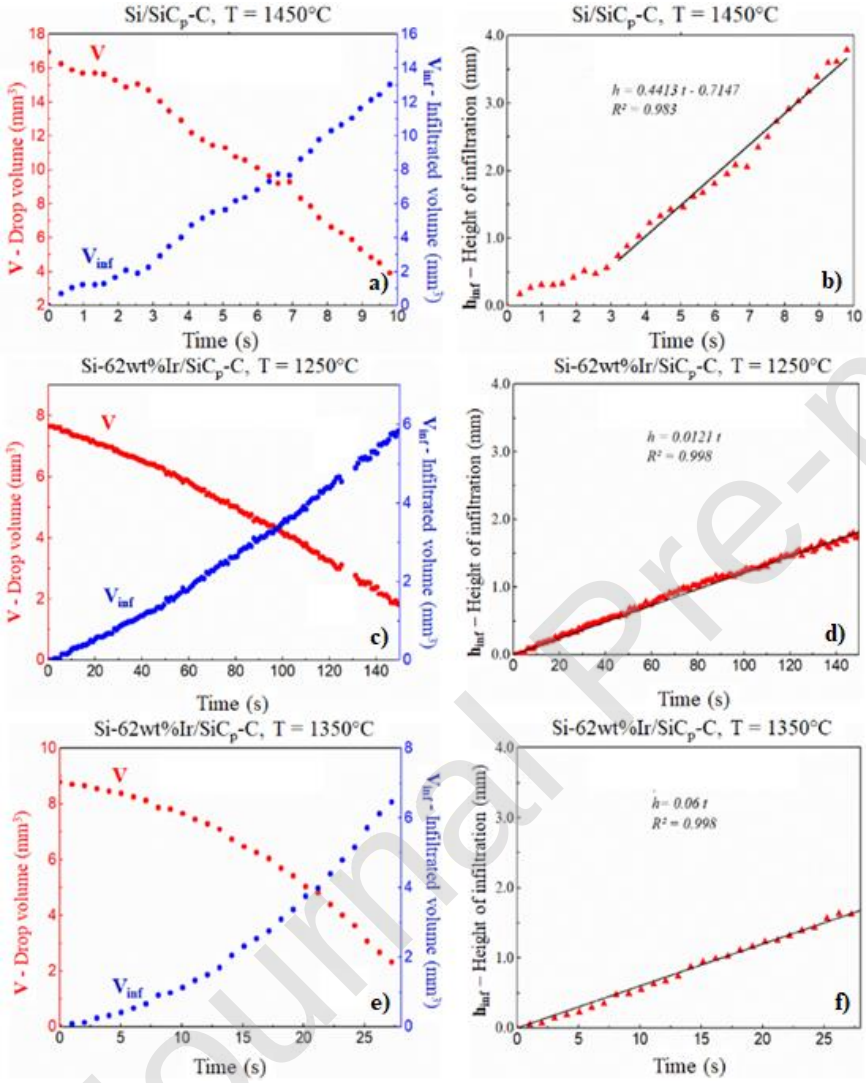

Fig. 7. Evolution of drop emerging volume (V), infiltrated volume (V_{inf}), and height of infiltration (h_{inf}) for experiments performed on SiC_p-C porous preforms by infiltrating: a) and b) pure Si at T = 1450°C; c) and d) Si-Ir eutectic alloy at T = 1250°C and e) and f) Si-Ir eutectic alloy at T = 1350°C. The linear equation and standard deviation are inserted.

The process of reactive infiltration is very complex, especially in this type of preforms, since there could be reactive and non-reactive infiltration mechanisms at the same time, The predominant mechanism depends on the C / SiC ratio. As proposed by [16] there may be up to 3 types of SiC: the first step is the C-dissolution by liquid Si (or even Si-based alloy), then the first SiC appears

(SiC type I) by reaction between Si and C. The as produced SiC grows epitaxially on the α-SiC. The second type of SiC can grow randomly (SiC type II) and the third one is produced as nano-sized particles when liquid Si undergoes to supersaturation by C (SiC type III) [16, 17]. The predominance of the different kinds of SiC produced largely depend on the process temperature and the type of C used. Indeed, it has been found that in the case of Si-Co alloys [23] and pure Si with different types of C, SiC type II and III [55] are present, while in the case of infiltration with Ni-Si alloys [56], SiC can only be seen from type II, but nucleating both in the surface of the pore and in the melt, while in the case of Al-Si, only SiC of the type II is also formed, but no growth is observed in the melt [55].

In Figure 8, SEM images of the cross-sectioned Si-infiltrated sample at T = 1450° C are shown.

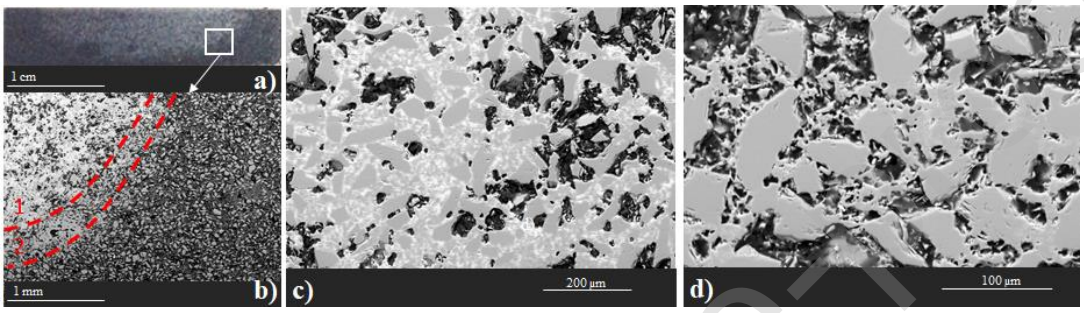

Fig. 8. BSE images of the microstructure after the infiltration of SiC_p-C preforms by pure Si at T = 1450°C: a) global infiltration area and b), c) and d) details of the resulting microstructure at higher magnifications in particular of infiltrated area 1 and 2.

Analyzing the infiltration front in Figure 8, two different infiltrated microstructures can be observed (area 1 and area 2, see Figure 8b). In particular, in the area 1 (Figure 8c), unreacted Si is still present (bright phase) surrounding the SiC particles. In parallel, as shown in Figure 8d, absence of unreacted Si is detected at the border of the infiltration front. This phenomenon has been previously observed, by infiltrating liquid Si into C with cylindrical pores of 500 µ. At the reaction front, a dense layer of SiC was detected [54]. . This evidence, together with the linear behavior of infiltration height as a function of time, let us to state that the reactivity is the main phenomenon controlling infiltration process. The same conclusion might be predicted when the infiltrating material is liquid Si-Ir eutectics. The final microstructure of SiC_p-C infiltrated with liquid Si-Ir eutectic alloy at T = 1250°C is shown in Figure 9. Owing to comparable size, it is not possible to distinguish between pre-existing SiC particles and new produced and growth SiC crystals by the reaction between Si and C during infiltration process [23]. A further evidence that infiltration was driven by reaction even for Si-Ir eutectic alloy, is the resulting activation energy. To calculate activation energy, some kinetic parameters need to be preliminarily determined, such

as the infiltration rate (U_{inf}). In Table 2 the values of infiltration rate (U_{inf}), spreading rate (U_{spred}) and their ratio itself, as a function of temperature and the metal material used, are reported.

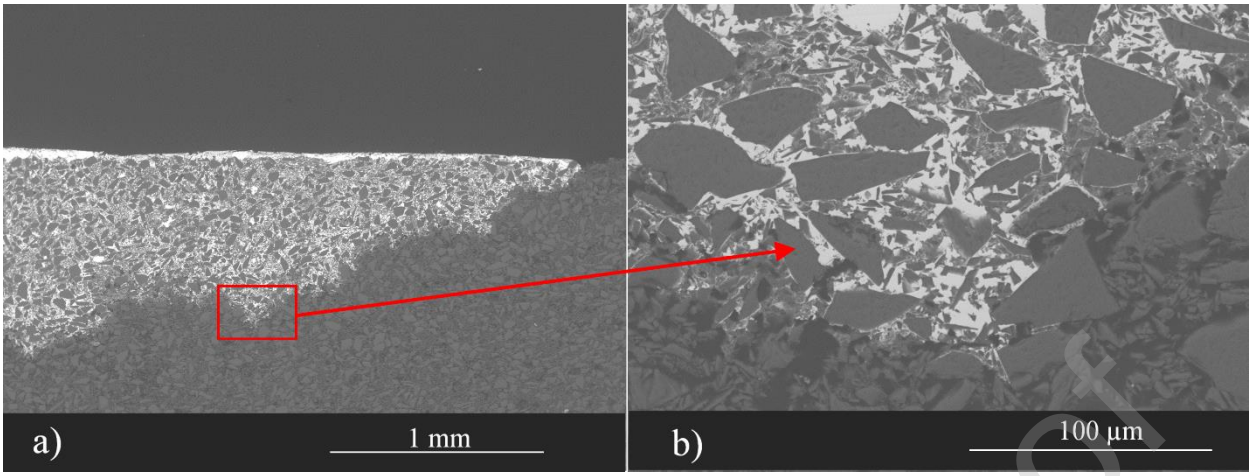

Fig. 9. BSE images of SiC_p-C preform microstructure infiltrated with liquid Si-Ir eutectic alloy at T = 1250°C. a) global microstructure of infiltrated area and b) detail of the infiltration front at higher magnification.

Tab. 2. Kinetic parameters (U_{inf}-infiltration and U_{spred}-spreading rates) calculated for infiltration experiments of SiC-C preforms with pure Si and Si-62wt.% Ir alloy, carried out at T = 1450°C, T = 1250°C and T = 1350°C, respectively.

Since the infiltration kinetics is linear with the time, the infiltration rate U_{inf} (= dh_{inf}/dt) is constant and equal to the slope of h_{inf} *(t)*. The spreading rate U_{esp} (= dR/dt) was calculated by the slope of the quasi-linear area of the curve R(t). Two aspects are deserving to be highlighted: as a first, the infiltration rate is greater of one order of magnitude than the value reported for graphite infiltrated with Ni-Si system [52, 56] even though the permeability is lower. Another important aspect deserving attention, although the tortuosity is greater than the value reported in [56], in all cases the infiltration rate is comparable or even higher than the spreading one.

By using Arrhenius equation and calculating the infiltration rate of Si-Ir eutectic alloy into SiC_p-C preform for two different temperatures, a value of the activation energy Ea_{inf} = 330 kJ/mol is resulting. For the sake of clarity, although Ea has been obtained from only two points, which is not very orthodox, the value obtained is reasonably acceptable by enlarging the tolerance interval from 200 to 400 kJ/mol. Despite the low precision of the data collected, the calculated Ea is in a good agreement with values around few hundred kJ/mol reported for reactive infiltration processes previously studied [56]. This range of Ea values discriminates between infiltration process driven by chemical reaction respect to infiltration driven by viscous resistance where the activation energy is usually resulting around tens of kJ/mol [60-62].

3.2 Microstructural characterization of the as produced composites

As aforementioned in the previous sections, SiC/Si and SiC/$IrSi_3$ composites were produced by Si and Si-62wt.% Ir eutectics infiltration into SiC_p-C preforms at T = 1450°C and T = 1350°C, respectively. In both cases metal infiltration took place spontaneously and complete infiltration of preforms were achieved within a dwell time of less than 5 min. At the end of the infiltration process, samples were removed from the furnace and abraded to remove the exceeding metal material.

As a first, the density of the as produced composites was measured and resulting 2.80 ± 0.05 g/cm^3 for SiC/Si and 6.35 ± 0.19 g/cm^3 for SiC/$IrSi_3$ (based on equipment accuracy) with a residual porosity of 4.9% and 6.4%, respectively.

SEM analyses on the cross-sectioned composite materials were performed. In Figure 10, the microstructures of the as produced SiC/Si and SiC/$IrSi_3$ composites are shown at different magnifications. At lower magnification, a high-dense microstructure with limited porosity is the first evidence: the pre-existing pores were completely filled by the metal material. Furthermore, no evidence of cracks or interface detachments between the matrix and reinforcement were detected, proving the excellent thermal compatibility between the phases.

Focusing on SiC/Si composite, by SEM/EDX (see Figures 10a and 10b), and X-ray diffraction (see Figure 11a), SiC (dark grey) and Si (bright) phases were detected. In addition, absence of unreacted C was either detected.

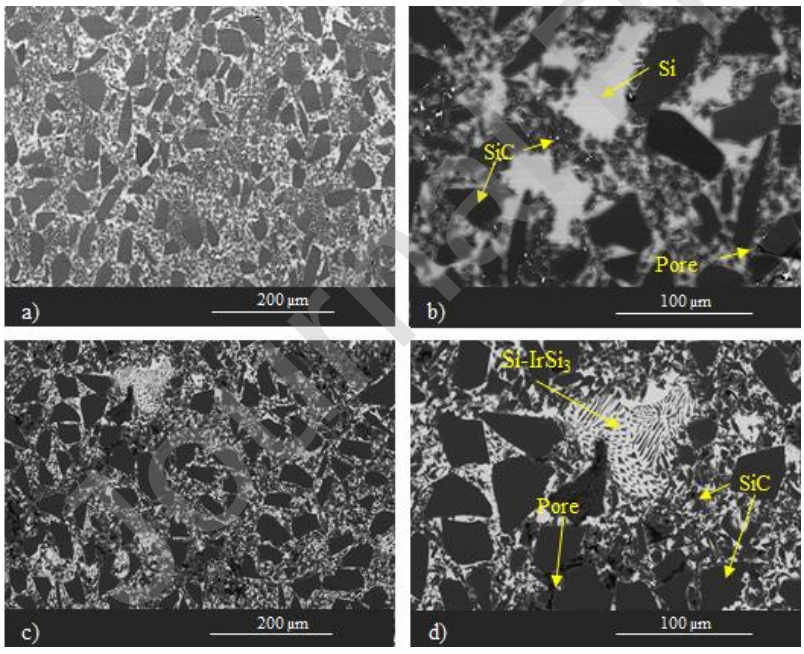

Fig. 10. SEM analyses (retro-scattered electrons) of cross-sectioned composite materials: a) and b) SiC/Si produced at T = 1450°C; and c) and d) SiC/$IrSi_3$ produced at T = 1350°C.

Regarding SiC/$IrSi_3$ composites, three different phases were detected by XRD (Figure 11b): SiC, Si and $IrSi_3$. SiC particles with three different sizes: 36.5, 4.5 and 1-2 μm (see Figures 10c and 10d). The SiC particles with lower size were produced during infiltration process (SiC type II) by reaction of Si with C. In the area surrounding the SiC particles, a Si-$IrSi_3$ eutectic phase is detected. Finally, as for SiC/Si, a residual porosity is still present into SiC/$IrSi_3$ produced composite.

As a general conclusion, both produced composites show a homogeneous highly-dense microstructure, key features to obtain high thermo-mechanical response.

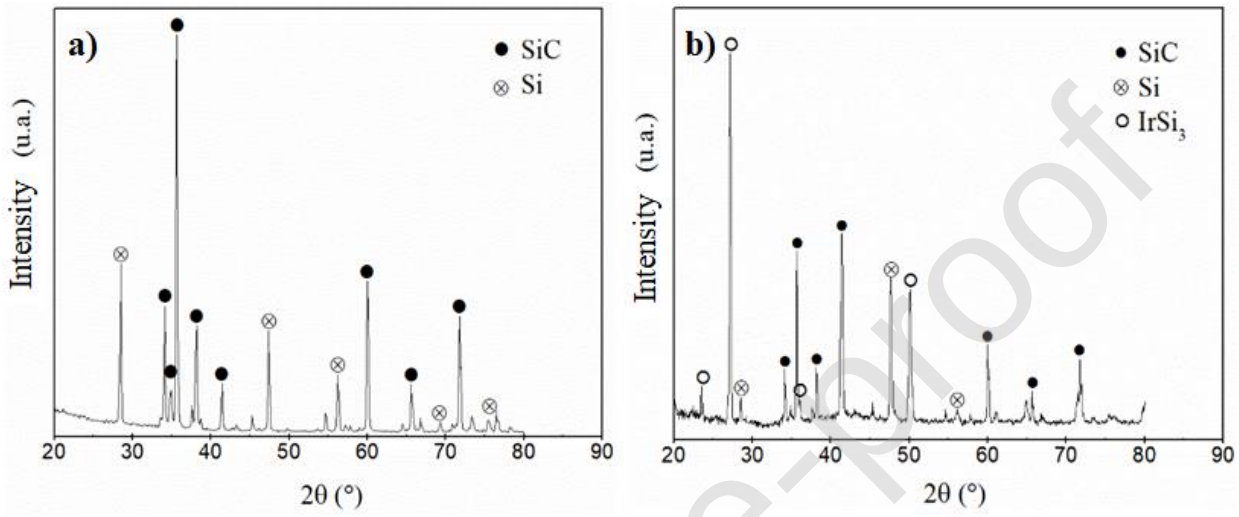

Fig. 11. X-ray diffraction patterns of composite materials: a) SiC/Si produced at T = 1450°C and b) SiC/$IrSi_3$ produced at T = 1350°C

4. Conclusions

For the first time, the feasibility to infiltrate SiC_p-C porous preforms (bimodal SiC particles bonded by C) by pure Si and Si-62wt%Ir eutectic alloy was successfully tested. For both the metal phases, the infiltrations of SiC_p-C preforms took place spontaneously and highly-dense, nearly-shaped SiC/Si and SiC/$IrSi_3$ composites were effortless produced. The presence of free C as bonding phase played a key role in driving the reactivity and kinetics within infiltration experiments. Since C is on the pore wall (bonding the bimodal SiC-particles) both infiltrations processes were mainly governed by SiC formation at the infiltration front.

Taking into account that:

1) the infiltration kinetics is well described by linear law;

2) the resulting activation energy is 300 ± 100 KJ/mol;

3) highly consolidated SiC particles is observed by the appearance of SiC type II;

let us to conclude that the infiltration process is mainly driven by reactivity.

However, the higher infiltration rate measured respect to similar experiments performed by infiltrating Si and Si-based alloys into porous graphite, together with the irregular infiltration fronts observed, suggests that capillarity and viscous forces might play a concomitantly role.

To better understand the overall infiltration process, a parallel investigation on the interactions at Si-Ir alloys/C-based materials interfaces by studying the wettability and spreading kinetics as a function of operating conditions is ongoing.

Declaration of interests

The authors declare that they have no known competing financial interests or personal relationships that could have appeared to influence the work reported in this paper.

The authors declare the following financial interests/personal relationships which may be considered as potential competing interests:

Acknowledgements

The work performed at the University of Alicante was funded by the Spanish "Ministerio de Economía y Competitividad" (Grant MAT2017-86992-R), and action Mobility of Alicante University. The work performed at CNR-ICMATE was supported by National Science Center of Poland through POLONEZ project number UMO-2016/23/P/ST8/01916. This project is carried out under POLONEZ-3 program which has received funding from European Union's Horizon 2020 research and innovation program under Marie Skłodowska-Curie grant agreement. No 665778.

DG wishes to thank Dr Vincenzo Buscaglia for the critical reading and his suggestions made to improve the manuscript. The authors would like to acknowledge Dr Massimiliano Valle (Petroceramics s.r.l) for kindly providing the SiC_p preforms used in this investigation.

References

[1] D.D.Chung, Composite Materials Science and Applications, Springer-Verlag London, 2010.

[2] I.M. Low, Ceramic Matrix Composites: Microstructure, Properties and Applications, Woodhead Publishing, 2006.

[3] R. Novakovic, B. Korthaus, Advanced Ceramics for Use in Highly Oxidizing and Corrosive Environments: Siliconised Silicon Carbide. Key Eng. Mater. 201 (2001) 141–182. https://doi.org/10.4028/www.scientific.net/KEM.201.141

[4] F. Cardarelli, Materials Handbook A Concise Desktop Reference, Springer-Verlag London, 2018.

[5] M. Srinivasan, Structural Ceramics, Academic Press, London, 1989.

[6] S. Prochazka, R.M. Scanlan, Effect of Boron and Carbon on sintering of SiC, J. Am. Ceram. Soc. 58 (1975) 72.

[7] F. Lange, T.K. Gupta, Sintering of SiC with boron compounds, J. Am. Ceram. Soc. 59 (1976) 537–538.

[8] J. Lis, Y. Miyamoto, R. Pampuch, K. Tanihata, Ti_3SiC-based materials prepared by HIP-SHS techniques, Mater. Lett. 22 (1995) 163–168. https://doi.org/10.1016/0167-577X(94)00246-0.

[9] E. Gomez, J. Echeberria, I. Iturriza, F. Castro, Liquid phase sintering of SiC with additions of Y_2O_3, Al_2O_3 and SiO_2, J. Eur. Ceram. Soc. 24 (2004) 2895–2903. https://doi.org/10.1016/j.jeurceramsoc.2003.09.002

[10] N. R. Calderon, M. Martinez-escandell, J. Narciso, F. Rodriguez-reinoso, Manufacture of biomorphic SiC components with homogeneous properties from sawdust by reactive infiltration with liquid silicon, J. Amer. Ceram. Soc. 93 (2010) 1003–1009. https://doi.org/10.1111/j.1551-2916.2009.03572.x

[11] N. R. Calderon, M. Martinez-escandell, J. Narciso, F. Rodriguez-reinoso, The combined effect of porosity and reactivity of the carbon preforms on the properties of SiC produced by reactive infiltration with liquid Si, Carbon 47 (2009) 2200–2210. https://doi.org/10.1016/j.carbon.2009.04.002

[12] N.R. Calderón, M. Martínez-Escandell, J. Narciso, F. Rodríguez-Reinoso, The role of carbon biotemplate density in mechanical properties of Biomorphic SiC, J. Eur. Ceram. Soc. 29 (3), (2009) 465-472.

[13] Y. Xie, L. Cheng, L. Li, H. Mei, L. Zhang, Strengthening/toughening of laminated SiC_w/SiC ceramic composites by heat treatment, Ceram. Int. 41 (2015) 10024–10029. https://doi.org/10.1016/j.ceramint.2015.04.087

[14] D. Kopeliovich, Advances in the manufacture of ceramic matrix composites using infiltration techniques. Advances in Ceramic Matrix Composites, 2014.

[15] S.T. Mileiko, Carbon/Carbon, Cement, and Ceramic Matrix Composites, Comprehensive Composite Materials, 2000.

[16] J.N. Ness, T.F. Page, Microstructural evolution in reaction-bonded silicon carbide, J. Mater. Sci. 21 (1986) 1377–1397.

[17] A.J. Whitehead, T.F. Page, Fabrication and characterization of some novel reaction-bonded silicon carbide materials, J. Mater. Sci. 27 (1992) 839–852.

[18] M. Caccia, J. Narciso, SiC manufacture via reactive infiltration, Processing and Properties of Advanced Ceramics and Composites VI: Ceramic Transactions, John Wiley & Sons, 2014.

[19] M. Caccia, J. Narciso, Production of SiC Materials by Reactive Infiltration, Mater. Sci. Forum 783–786 (2014) 1863–1866. https://doi.org/10.4028/www.scientific.net/MSF.783-786.1863

[20] J.F. Narciso-Romero, R. Arpón-Carballo, Synthesis of mixed disilicides/SiC composites by displacement reaction between metal carbides and silicon, J. Ceram. Soc. Jpn. 108 (2000) 957–959. https://doi.org/10.1016/j.msea.2004.03.052

[21] D. Y. Oh, H. C. Kim, J. K. Yoon, I. Ko, I. J. Shon, One step synthesis of dense $MoSi_2$-SiC composite by high-frequency induction heated combustion and its mechanical properties, J. Alloy Comp. 395 (1-2) (2005) 174–180. https://doi.org/10.1016/j.jallcom.2004.10.072
[22] M. Caccia, C. Xiang, J. Narciso, N. Gupta, Reactive melt infiltration as synthesis route for enhanced SiC/$CoSi_2$ composite materials for advanced armor systems, Ceram. Int. 44 (11) (2018) 13182-13190. https://doi.org/10.1016/j.ceramint.2018.04.143
[23] M. Caccia, S. Amore, D. Giuranno, E. Ricci, J. Narciso, Towards optimization of SiC/$CoSi_2$ composite material manufacture via reactive infiltration: Wetting study of Si–Co alloys on carbon materials, J. Eur. Ceram. Soc. 35 (15) (2015) 4099-4106. https://doi.org/10.1016/j.jeurceramsoc.2015.07.016
[24] O. C. Esteban, M. Caccia, A. Camarano, J. Narciso, Advances in High Temperature Ceramic Matrix Composites and Materials for Sustainable Development; Ceramic Transactions, John Wiley & Sons, 2017.
[25] P. J. Meschter, D. S. Schwartz, Silicide-matrix materials for high-temperature applications, J. Miner. Met. Mater. Soc. 41(1989) 52–55. https://doi.org/10.1007/BF03220384
[26] B. E. K. Ohriner, Processing of iridium and iridium alloys, Platin. Met. Rev. 52 (2008)186–197. doi:10.1595/147106708x333827.
[27] I. Iavicoli, V. Leso, Iridium. Handbook on the Toxicology of Metals (eds. G. Nordberg, B. Fowler, M. Nordberg, Academic Press, 2014). https://doi.org/10.1016/C2011-0-07884-5
[28] R. Crabtree, Iridium compounds in catalysis, Acc. Chem. Res. 12 (9) (1979) 331–337. doi: 10.1021/ar50141a005
[29] S. B. Singh, Green Chemistry & Technology Letters 2 (4) (2016) 206-210. doi: 10.18510/gctl.2016.247
[30] W.D. Huang, H. Cao, S. Deb, M. Chiao, J.C. Chiao, Iridium oxide based coaxial pH ultramicroelectrode, Sensors and Actuators A 169 (2011) 1-11. https://doi.org/10.1016/j.elecom.2013.12.012
[31] S. Vasudevan, Anodes for Electrochemcial Processes (Part-I), Res. J. Chem. Sci 3 (5) (2013) 1-2.
[32] D. R. Lide, CRC Handbook of Chemistry and Physics. (CRC Press, 2010).
[33] Y. Y. Mitarai, Y. Ro, T. Maruko, H. Harada, Ir-base refractory superalloys for ultra-high temperatures, Met. Mat. Trans. A 29 (1998) 537-549. https://doi.org/10.1007/s11661-998-0135-9
[34] K. Mumtaz, J. Echigoya, M. Taya, Thermal cycling of iridium coatings on isotropic graphite, J. Mater. Sci. 28 (1993) 5521–5527. https://doi.org/10.1007/BF00354413
[35] J. R. Strife, J. G. Smeggil, W. L. Worrell, Reaction of Iridium with Metal Carbides in the Temperature Range of 1923 to 2400 K, J. Am. Ceram. Soc. 73 (1990) 838–845. https://doi.org/10.1111/j.1151-2916.1990.tb05123.x
[36] National Research Council. High-Temperature Oxidation-Resistant Coatings: Coatings for Protection From Oxidation of Superalloys, Refractory Metals, and Graphite. (The National Academies Press, 1970).
[37] Y. Huang, S. Bai, H. Zhang, Y. Ye, L. Zhu, Oxidation of Iridium coatings on rhenium substrates at ultrahigh temperature in stagnant air: its failure mechanism and life model, Surf. Coatings Technol. 288, (2016) 52–61. https://doi.org/10.1016/j.surfcoat.2016.01.004
[38] Z. Chen, Iridium Coating: Processes, Properties and Application. Part I. Johnson Matthey Technol. Rev. 61 (2017) 16–28. http://dx.doi.org/10.1595/205651317X693606
[39] K. L. Luthra, US Patent - N 5,080,862 - Iridium Silicon alloy. (1992).
[40] S. T. Prisbrey, US Patent, N 6,759,141 - Oxidation preventative capping layer for deep-ultra-violet and soft x-ray multilayers. 1 (2004).
[41] S. Prisbey, S. Vernon, Iridium/Iridium Silicide as an oxidation rsistant Capping Layer for soft X-ray Mirrors, UCRL-CONF-203395 (2004).

[42] F.M. d'Heurle, the oxidation of silicides on silicon, The Physics and Chemistry of SiO_2 and the Si-SiO2 interface, edited b B.E. Deal & C.R. Helms, Springer, (1988), 85-94.
[43] A. Camarano, J. Narciso, D. Giuranno, Solid state reactions between SiC and Ir, J.Eur. Ceram. Soc. 39 (4) (2019) 3959-3970.
[44] C. A. Swenson, Recommended Values for the Thermal Expansivity of Silicon from 0 to 1000 K, J. Phys. Chem. Ref. Data 12 (1983) 179–182. https://doi.org/10.1063/1.555681
[45] J. J. Halvorson, R. T. Wimber, Thermal Expansion of Iridium at High Temperatures, J. Appl. Phys. 43 (1972) 2519–2522.
[46] Z. Li, R. C. Bradt, Thermal expansion of the cubic (3C) polytype of SiC, J. Mater. Sci. 21 (1986) 4366–4368. doi: 10.1007/BF01106557
[47] H. Okamoto, Ir-Si (Iridium-Silicon). J. Phase Equilibria Diffus. 28 (2007) 495. doi: 10.1007/s11669-007-9151-5
[48] Petroceramic. Available at: http://www.petroceramics.com/
[49] M. Caccia, J. Narciso, Key Parameters in the Manufacture of SiC-Based Composite Materials by Reactive Infiltration, Materials (2019).
[50] M. Caccia, J. Narciso, On the effects of hot spot formation during MW-assisted synthesis of Cf/SiC composites by reactive melt infiltration: Experimental simulations through high temperature treatments, J.Eur. Cearm. Soc. 40 (1) (2019) 28-35.
[51] R. Novakovic, E. Ricci, D. Giuranno, T. Lanata, S. Amore, Thermodynamics and surface properties of liquid Bi-In alloys, Calphad 33 (1) (2009) 69-75.
[52] M. Caccia, D. Giuranno, J.M. Molina, M. Moral, R. Nowak, E. Ricci, N. Sobczak, J. Narciso, J.F. Sanz, Graphene Translucency and Interfacial Interactions in the Gold/Graphene/SiC System, J. Phys. Chem. Let. 9 (14) (2018) 3850-3855.
[53] M. Caccia, A. Camarano, D. Sergi, A. Ortona, J. Narciso, Wetting and Navier-Stokes Equation — The Manufacture of Composite Materials, Wetting and Wettability (ed. by M. Aliofkhazraei, Intech, 105-138, 2015).
[54] D. Sergi, A. Camarano, J.M. Molina, A. Ortona, J. Narciso, Surface growth for molten silicon infiltration into carbon millimeter-sized channels: Lattice-Boltzman simulations, experiments and models, International Journal of Modern Physics C 27 (06), (2016) 1650062.
[55] N. R. Calderon, R. Voytovych, J. Narciso, N. Eustathopoulos, Pressureless infiltration versus wetting in AlSi/graphite system, J. Mater. Sci. 45 (2010) 4345–4350.
[56] V. Bougiouri, R. Voytovych, N.Rojo-Calderon, J.Narciso, N. Eustathopoulos, The role of the chemical reaction in the infiltration of porous carbon by NiSi alloys, Scr. Mater. 54 (2006) 1875–1878.
[57] V. M. Starov, S. A.Zhdanov, S. R. Kosvintsev, V. D. Sobolev, M. G.Velarde, Adv. Colloid Interface Sci. 104 (2003) 123–158.
[58] A. Clarke, T. D. Blake, K. Carruthers, A.Woodward, Spreading and Imbibition of Liquid Droplets on Porous Surface, Langmuir 18 (2002) 2980–2984.
[59] H. R. Charles-Williams, R. Wengeler, K. Flore, H. Feise, M.J. Hounslow, A.D. Salman, Granule nucleation and growth: Competing drop spreading and infiltration processes, Powder Technol. 206 (2011) 63–71.
[60] C. Garcia-Cordovilla, E. Louis, J. Narciso, Pressure infiltration of packed ceramic particulates by liquid metals, Acta Mater. 47 (1999) 4461–4479.
[61] N.R. Calderon, R. Voytovych, J Narciso, N Eustathopoulos, Wetting dynamics versus interfacial reactivity of AlSi alloys on carbon, J. Mater. Sci. 45 (8), (2010) 2150-2156.
[62] R. Israel, R. Voytovych, P. Protsenko, B. Drevet, D. Camel, N. Eustathopoulos, Capillary interactions between molten silicon and porous graphite, J. Mater. Sci. 45 (2010) 2210–2217.
[62]

Tab. 1. Main characteristics of SiC_p-C Petroceramic preform.

Property		**Value**	**Unit**
Density	Apparent density	2,10-2,20	g/cm^3
	Helium density	3,10	g/cm^3
Porosity	Porosity (α_{ef})	30,6	%
	Medium pore diameter	1,3	µm
Composition	Silicon carbide (α-SiC)	95,3	wt.%
	Carbon binder (C)	4,7	wt.%

Tab. 2. Kinetic parameters (U_{inf}-infiltration and U_{spred}-spreading rates) calculated for infiltration experiments of SiC-C preforms with pure Si and Si-62wt.% Ir alloy, carried out at T = 1450°C, T = 1250°C and 1350°C, respectively.

Metal	**T (°C)**	**U_{inf} (µm/s)**	**U_{esp} (µm/s)**	**U_{inf} / U_{esp}**
Si	1450	375,0	33,4	11,2
Si-62wt.%Ir	1250	12,1	7,0	1,73
Si-62wt.%Ir	1350	60,1	49,2	1,22